Chemical Science

ROYAL SOCIETY OF CHEMISTRY

EDGE ARTICLE

View Article Online
View Journal | View Issue

Cite this: *Chem. Sci.*, 2026, **17**, 4998

All publication charges for this article have been paid for by the Royal Society of Chemistry

Toward photodynamic detection and photodynamic therapy of tumours over-expressing carbonic anhydrase IX with a phosphorescent organometallic iridium(III) antibody conjugate

Emily R. McGowan, [a] Stacey E. Rudd, [a] Katherine A. Morgan, [a] Trevor A. Smith [b] and Paul S. Donnelly *[a]

Antibody conjugates with phosphorescent organometallic iridium(III) complexes attached to tumour targeting antibodies have the potential to be used as emissive probes to guide surgical resection of tumours and for tumour-targeted photodynamic therapy. In this work, a bidentate 2-pyridyl-1,2,3-triazole ligand with a polyethylene glycol linker and a squaramide ethyl ester functional group has been used as an ancillary ligand to make phosphorescent iridium(III) complexes. The excitation and emission energies for the iridium(III) complexes were tuned to lower energy by increasing the aromatic conjugation in the cyclometalating ligands. The squaramide ethyl ester functional group is used to attach the iridium(III) complexes to girentuximab, an antibody that binds to carbonic anhydrase IX (CAIX). Over-expression of carbonic anhydrase IX is a characteristic of several tumour types, including clear cell renal cell carcinoma, glioblastoma, triple-negative breast cancer, ovarian cancer, and colorectal cancer. The squaramide ethyl ester functional group reacts with lysine residues in girentuximab to attach the iridium(III) complexes through stable vinylogous amide linkages. The cellular uptake of one iridium(III)-girentuximab conjugate was demonstrated using confocal microscopy and the conjugate is not toxic to HT-29 cells that over express CAIX, but irradiation with visible light results in dose dependent cytotoxicity. The iridium(III)-girentuximab conjugate described here could be of use for emissive detection of carbonic anhydrase IX positive tumour tissue to guide surgical resection as well as carbonic anhydrase IX targeted photodynamic therapy. The approach described here could be used with other tumour targeting antibodies.

Received 6th October 2025
Accepted 25th December 2025

DOI: 10.1039/d5sc07715j

rsc.li/chemical-science

Introduction

Surgical resection of solid tumours requires the surgeon to accurately identify all cancerous tissue to minimise the potential for metastasis and reoccurrence. Fluorescent molecules can be used to improve visualisation of tumour tissue and guide surgical resection.[1,2] Fluorescence guided surgery has often involved the use of simple dyes such as fluorescein and indocyanine dyes that lack specificity for diseased tissue. Recent interest has focused on molecularly targeted fluorescent probes that selectively bind to receptors or enzymes over-expressed in tumour tissue.[3,4]

Technological advances have seen an increase in the use of robotic-assisted surgery where a surgeon controls robotic arms to perform surgery through small incisions. The use of robotic arms to manipulate the surgical instruments allows for greater precision and dexterity to support minimally invasive procedures. Robot-assisted surgery has found application in prostate cancer (urology) but is also increasingly being adopted in gynaecology and general surgery. Robotic surgery systems often incorporate drop-in gamma detectors and endoscopic vision equipped with white light imaging and fluorescence imaging capabilities to support image-guided surgical resection.[1,5] Most robot-assisted clinical studies have involved the use of gamma-emitting technetium-99^{m} tracers or traditional organic fluorophores such as fluorescein, indocyanine green, sulfo-Cy5 and IRDye800CW.[6–8] Phosphorescent organometallic iridium(III) complexes can be prepared containing two cyclometalating bidentate ligands (C^N) such as 2-phenylpyridine (ppy) or 1-phenylisoquinoline (piq) and one bidentate 'ancillary ligand' (Fig. 1). Potential advantages of phosphorescent iridium(III) complexes when compared to traditional organic fluorophores include: relatively large Stokes shifts that can reduce inner filter effects, long phosphorescence lifetimes and a high degree of resistance to photo-bleaching.[9] Strong spin–orbit coupling in iridium(III) complexes, due to the presence of the heavy metal atom, promotes intersystem crossing and population of triplet metal to ligand charge transfer states (^{3}MLCT)

[a]*School of Chemistry and Bio21 Molecular Science and Biotechnology Institute, University of Melbourne, Melbourne, Victoria 3010, Australia. E-mail: pauld@unimelb.edu.au*

[b]*School of Chemistry, University of Melbourne, Melbourne, Victoria 3010, Australia*

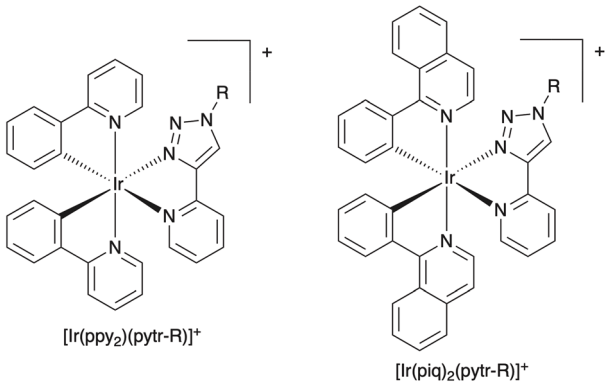

Fig. 1 Chemical structures of organometallic complexes containing two cyclometalating ligands, either ppy or piq, and one 2-pyridyl-1,2,3-triazole ancillary ligand.

that result in emission with relatively long phosphorescent emission lifetimes. The ^{3}MLCT excited state can interact with oxygen to form cytotoxic singlet oxygen ($^1O_2$) leading to potential for Photodynamic Therapy (PDT).[9–11]

PDT involves activation of a molecule, called a photosensitiser, by light in the presence of oxygen to initiate a therapeutic effect. PDT is used to treat certain forms of cancer, some skin conditions and age-related macular degeneration. It is feasible that robotic surgery equipment could be augmented for the endoscope camera to involve fibre optic lasers that could be used for minimally invasive photodynamic therapy to be coupled with photodynamic detection.[1] One of the advantages of photodynamic therapy when compared to traditional chemotherapy is that the photosensitiser, light and oxygen are all individually innocuous but combine when co-located to kill tumour cells and, in some instances, even invoke an immune response.[12,13] The mechanism of action of PDT is a complicated process but generally falls into two categories: type I processes involve photoinduced electron transfer to form superoxide ($O_2^{\bullet-}$) or hydroperoxyl radicals ($HO_2^{\bullet}$); type II involves energy transfer from the photosensitiser to ground state oxygen ($^3O_2$) to form singlet oxygen ($^1O_2$).[14] The first photosensitiser to get clinical approval for the treatment of bladder cancer was an ill-defined mixture of porphyrin polymers called Photofrin. For metal-free porphyrin-based sensitisers, such as Photofrin, $^1O_2$ formation relies on population of π–π* excited states of Photofrin for direct interaction with molecular oxygen and overall efficacy is limited by a relatively short-lived excited state and rapid photobleaching. In contrast to purely organic photosensitisers, iridium(III) complexes offer many different excited-state electronic configurations that can be exploited in oxygen independent and oxygen dependent pathways.

An attractive property of iridium(III) luminescent complexes is the ability to tune the emissive properties by manipulation of either the cyclometalating ligand or ancillary ligand.[15] In our previous work, we prepared a family of iridium(III) complexes with substituted 1,2,3-triazole ligands with reactive functional groups that react with either cysteine or lysine residues of the metalloprotein transferrin to fluorescently label the protein.[16] In seeking to extend this work to tumour targeting antibodies we found attaching these relatively hydrophobic iridium(III) complexes to antibodies induced unwanted aggregation and compromised biological activity. In this work, a new bidentate 2-pyridyl-1,2,3-triazole ligand with a relatively long polyethylene glycol linker (PEG_7) with a terminal squaramide ethyl ester functional group is used to make phosphorescent iridium(III) complexes. The squaramide ethyl ester functional group reacts selectively with lysine residues present in antibodies at room temperature and in aqueous solutions to form stable aromatic vinylogous diamide linkages to the antibody.[17–20] The new iridium(III) complexes were reacted with girentuximab, an antibody that selectively binds to carbonic anhydrase IX. Over-expression of carbonic anhydrase IX is a characteristic of several tumours, including clear cell renal cell carcinoma, glioblastoma, triple-negative breast cancer, ovarian cancer, and colorectal cancer. Girentuximab radiolabelled with either zirconium-89 or lutetium-177 is under investigation for diagnostic imaging and radioimmunotherapy of CAIX positive tumours.[21–23] The goal of this research was to take advantage of the tumour targeting properties of the antibody to generate new tumour targeting phosphorescent metal complexes with potential application in both photodynamic detection and photodynamic therapy.

Results and discussion

Synthesis

A bidentate 2-pyridyl-1,2,3-triazole ligand with a $-((CH_2)_2O)_7(CH_2)_2NH_2$ functional group (pytr-NH_2) was synthesised by a copper-catalysed azide–alkyne cycloaddition reaction between azido-PEG_7-amine and 2-ethynylpyridine in a mixture of water and tetrahydrofuran (Scheme 1). The new ligand was then reacted with either $[Ir(ppy)_2(\mu\text{-}Cl)]_2$ or $[Ir(piq)_2(\mu\text{-}Cl)]_2$ to form the organometallic complexes $[Ir(ppy)_2(pytr\text{-}NH_2)]^+$ and $[Ir(piq)_2(pytr\text{-}NH_2)]^+$ respectively (Scheme 1). Both complexes were purified by reversed-phase high performance liquid chromatography (RP-HPLC). The amine functional group in both $[Ir(ppy)_2(pytr\text{-}NH_2)]^+$ and $[Ir(piq)_2(pytr\text{-}NH_2)]^+$ was reacted with diethyl squarate in a reaction heated with microwave irradiation. Purification by RP-HPLC allowed isolation of $[Ir(ppy)_2(pytr\text{-}SqOEt)]^+$ and $[Ir(piq)_2(pytr\text{-}SqOEt]^+$ as yellow and red solids respectively. All the new complexes were characterised by ^{1}H and ^{13}C NMR spectroscopy, electrospray ionisation mass spectrometry and analytical RP-HPLC. In the ^{1}HNMR spectra for all four complexes, the triazole proton signal is observed at 9.0 ppm. Esterification to the -SqOEt complexes is confirmed by the appearance of a triplet at 1.3 ppm, assigned to the CH_3 group of the squaramide ethyl ester. While formic acid (0.1%) was used in the RP-HPLC purification of some of the prepared complexes, the absence of signals corresponding to formate counterions in the ^{1}H and ^{13}C NMR spectra leads us to presume that the counterion is a hydroxide ion.[24]

Electronic properties of $[Ir(C\hat{}N)_2(pytr\text{-}NH_2)]^+$ and $[Ir(C\hat{}N)_2(pytr\text{-}SqOEt)]^+$

The UV/visible absorption spectra of solutions of the complexes with ppy as a cyclometalating ligand, $[Ir(ppy)_2(pytr\text{-}NH_2)]^+$ and

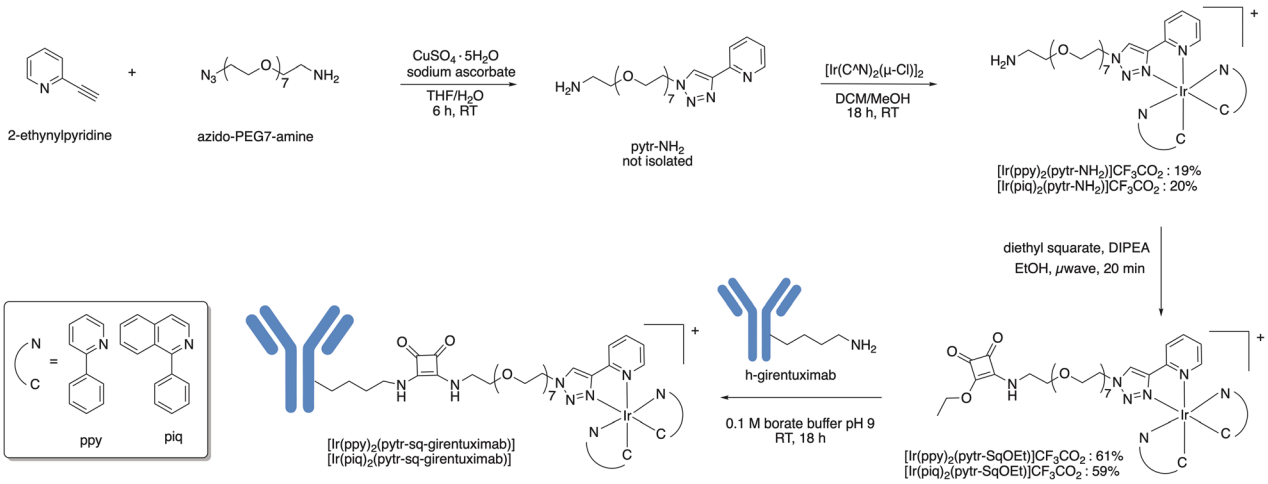

Scheme 1 Synthesis of $[Ir(ppy)_2(pytr\text{-}SqOEt)]^+$ and $[Ir(piq)_2(pytr\text{-}SqOEt)]^+$, and conjugation of $[Ir(C\text{^}N)_2(pytr\text{-}SqOEt)]^+$ to girentuximab by reaction of the squaramide ethyl ester functional group with amines of lysine residues to form squaramide linkages.

$[Ir(ppy)_2(pytr\text{-}SqOEt)]^+$, have maxima in the UV region (λ_{abs} = 254 nm, ε = 41 000 for $-NH_2$; λ_{abs} = 258 nm, ε = 61 000 for -SqOEt) due to π–π^* ligand centred (^{1}LC) transitions as well as maxima tailing into the visible region at λ_{abs} = 380 nm (ε = 4000 M^{-1} cm^{-1} for $-NH_2$, 4400 for -SqOEt) due to Metal to Ligand Charge Transfer (^{1}MLCT and ^{3}MLCT) transitions (Fig. 2a). Both $[Ir(ppy)_2(pytr\text{-}NH_2)]^+$ and $[Ir(ppy)_2(pytr\text{-}SqOEt)]^+$ are phosphorescent with emission at λ_{em} = 480 nm (λ_{ex} = 380 nm) with vibronic structure consistent with mixing of ^{3}LC and ^{3}MLCT excited states similar to what has been reported with other iridium(III) complexes with pyridyl-1,2,3-triazole ancillary ligands.[15,25,26] The extended aromatic conjugation in the complexes with a piq cyclometalating ligand, $[Ir(piq)_2(pytr\text{-}NH_2)]^+$ and $[Ir(piq)_2(pytr\text{-}SqOEt)]^+$, has a dramatic effect on the energy of the MLCT transitions and large bathochromic shifts to λ_{abs} = 435 nm (Fig. 2b) tailing to ~500 nm are observed. $[Ir(piq)_2(pytr\text{-}NH_2)]^+$ and $[Ir(piq)_2(pytr\text{-}SqOEt)]^+$ are phosphorescent with large Stokes shifts and emission centred at λ_{em} = 590 nm (λ_{ex} = 435 nm). Preliminary experiments show that it is possible to stimulate emission from both $[Ir(ppy)_2(pytr\text{-}NH_2)]^+$

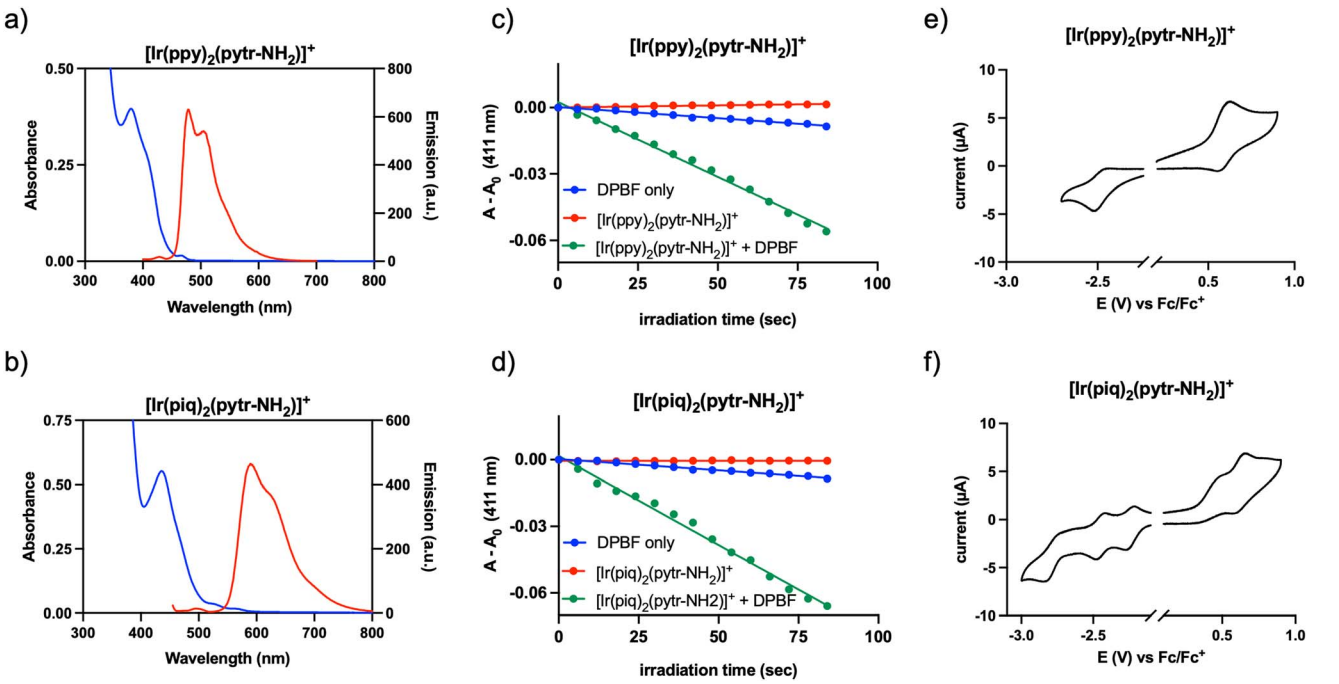

Fig. 2 (a) and (b) MLCT absorbance (blue) and emission (red) spectra of $[Ir(ppy)_2(pytr\text{-}NH_2)]^+$ and $[Ir(piq)_2(pytr\text{-}NH_2)]^+$ in acetonitrile. (c) and (d) plot of A–A_0 at 411 nm for DPBF (10 μM, blue) $[Ir(ppy)_2(pytr\text{-}NH_2)]^+$ or $[Ir(piq)_2(pytr\text{-}NH_2)]$ only (red), and DPBF with $[Ir(ppy)_2(pytr\text{-}NH_2)]^+$ or $[Ir(piq)_2(pytr\text{-}NH_2)]$ (green). (e) and (f) Cyclic voltammograms of $[Ir(ppy)_2(pytr\text{-}NH_2)]^+$ and $[Ir(piq)_2(pytr\text{-}NH_2)]^+$, in acetonitrile, 200 mV s^{-1}, potentials quoted *versus* ferrocenium/ferrocene.

and $[Ir(piq)_2(pytr\text{-}NH_2)]^+$ using two photon excitation ($\lambda_{exc} = 800$ nm) (Fig. S21). Excited state lifetimes were measured for $[Ir(ppy)_2(pytr\text{-}NH_2)]^+$ and $[Ir(piq)_2(pytr\text{-}NH_2)]^+$ in degassed acetonitrile and were 2.65 μs and 3.58 μs respectively.

The ability of $[Ir(C\text{^}N)_2(pytr\text{-}NH_2)]^+$ to generate singlet oxygen following activation by light ($\lambda = 365$ nm) was measured in aerated acetonitrile using 1,3-diphenylisobenzofuran (DPBF) as a chemical trap for $^1O_2$. Solutions of the $[Ir(C\text{^}N)_2(pytr\text{-}NH_2)]^+$ complexes (A_{365} 0.1–0.2) with DPBF (10 μM) were subject to irradiation with light ($\lambda = 365$ nm). The decrease in absorption at $\lambda = 411$ nm was measured and plotted against cumulative irradiation time (Fig. 2). For the phenylpyridine complex the singlet oxygen quantum yield was 0.58 while for the phenylisoquinoline complex it was 0.87. ($[Ru(bpy)_3]Cl_2$ was used as a reference, $\Phi_\Delta = 0.57$ in aerated CH_3CN).

Assays with the spectroscopic probes hydroxyphenyl fluorescein (HPF) and dihydrorhodamine 123 (DHR123) suggested that irradiation of solutions of either $[Ir(ppy)_2(pytr\text{-}NH_2)]^+$ or $[Ir(piq)_2(pytr\text{-}NH_2)]^+$ also leads to the generation of hydroxyl radicals ($^{\bullet}OH$) and superoxide anion radicals ($^{\bullet}O_2^-$) (Fig. S15 and S16).[27] The photogeneration of hydroxyl radicals and superoxide anion radicals as well as singlet oxygen suggests the complexes have potential to be cytotoxic through both type I and type II processes.

The electrochemical properties of $[Ir(ppy)_2(pytr\text{-}NH_2)]^+$ and $[Ir(piq)_2(pytr\text{-}NH_2)]^+$ were investigated by cyclic voltammetry. For quasi-reversible processes mid-point potentials ($E_m = (E_{pa} - E_{pc})/2$) are reported and the peak potentials (E_p) are reported for irreversible processes. For $[Ir(ppy)_2(pytr\text{-}NH_2)]^+$ a quasi-reversible process at $E_m = 0.60$ V (*vs.* Fc^+/Fc, $i_{pc}/i_{pa} = 0.06$) is attributed to the $Ir^{IV/III}$ redox couple (Fig. 2e). A similar $Ir^{IV/III}$ process $E_m = 0.62$ V ($i_{pc}/i_{pa} = 0.1$) is present in the cyclic voltammogram of $[Ir(piq)_2(pytr\text{-}NH_2)]^+$ as well as a broad poorly resolved irreversible process at $E_m = 0.49$ V (Fig. 2f). A quasi-reversible process at $E_m = -2.50$ V ($i_{pa}/i_{pc} = 0.08$) in the cyclic voltammogram of $[Ir(ppy)_2(pytr\text{-}NH_2)]^+$ is attributed to a ligand-based reduction. For the complex with phenylisoquinoline cyclometalating ligands, $[Ir(piq)_2(pytr\text{-}NH_2)]^+$, two quasi-reversible reductions at $E_m = -2.2$ ($i_{pa}/i_{pc} = 0.42$) and -2.4 ($i_{pa}/i_{pc} = 0.16$) are tentatively assigned to sequential population of the π^* orbital on each piq ligand. An irreversible process at even more negative potential, $E_p = -2.8$ V is tentatively attributed to reduction of the pyridyl functional group of the triazole ancillary ligand.[15,28]

Synthesis of $[Ir(C^N)_2(pytr\text{-}Sq\text{-}girentuximab)]$

Either $[Ir(ppy)_2(pytr\text{-}SqOEt)]^+$ or $[Ir(piq)_2(pytr\text{-}SqOEt)]^+$ (20 equivalents) were reacted with girentuximab in borate buffer (pH 9.0) for 18 hours to allow the squaramide ethyl ester functional group to react with amine groups on the side chains of solvent accessible lysine residues of the antibody (Scheme 1). Unreacted iridium(III) complex was removed by size exclusion chromatography and the purity of the conjugates was confirmed by size exclusion chromatography (Fig. S13).

After 18 h at room temperature, intact protein ESI-MS of the $[Ir(ppy)_2(pytr\text{-}Sq\text{-}girentuximab)]$ conjugate showed a distribution of between one and six additions of the complex per antibody with an estimated average of 3.6 additions per antibody (Fig. S20). An intact protein ESI-MS spectrum of the $[Ir(piq)_2(pytr\text{-}Sq\text{-}girentuximab)]$ could not be obtained, but we assume a similar complex to antibody ratio. The binding of $[Ir(ppy)_2(pytr\text{-}Sq\text{-}girentuximab)]$ and $[Ir(piq)_2(pytr\text{-}Sq\text{-}girentuximab)]$ to CAIX was analysed by an Enzyme-Linked Immunosorbent Assay (ELISA, Fig. 3). The EC_{50} values for the $[Ir(ppy)_2(pytr\text{-}Sq\text{-}girentuximab)]$ (1.7 nM) and $[Ir(piq)_2(pytr\text{-}Sq\text{-}girentuximab)]$ (1.5 nM) are similar to that of unconjugated girentuximab (0.8 nM), indicating that the girentuximab conjugates retain binding affinity for CAIX. The absorption spectra of $[Ir(ppy)_2(pytr\text{-}Sq\text{-}girentuximab)]$ and $[Ir(piq)_2(pytr\text{-}Sq\text{-}$

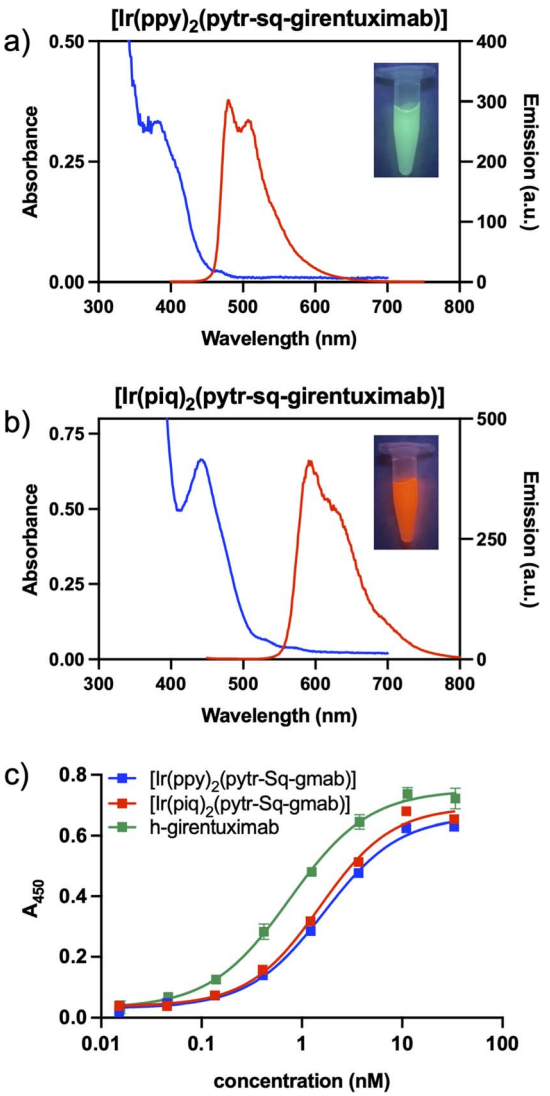

Fig. 3 (a) Absorbance (blue) and emission ($\lambda_{ex} = 380$ nm, red) spectra of $[Ir(ppy)_2(pytr\text{-}Sq\text{-}girentuximab)]$ in 0.9% saline. Inset: $[Ir(ppy)_2(pytr\text{-}Sq\text{-}girentuximab)]$ under UV irradiation ($\lambda_{ex} = 365$ nm). (b) absorbance (blue) and emission ($\lambda_{ex} = 435$ nm, red) spectra of $[Ir(piq)_2(pytr\text{-}Sq\text{-}girentuximab)]$ in 0.9% saline. Inset: $[Ir(piq)_2(pytr\text{-}Sq\text{-}girentuximab)]$ under UV irradiation ($\lambda_{ex} = 365$ nm). (c) ELISA curves for girentuximab, $[Ir(ppy)_2(pytr\text{-}Sq\text{-}girentuximab)]$, and $[Ir(piq)_2(pytr\text{-}Sq\text{-}girentuximab)]$ (gmab = girentuximab).

girentuximab)] are similar to the unconjugated complexes and the antibody conjugates also retain the phosphorescence properties with two broad maxima at $\lambda_{em} = 480$ and 505 nm, and $\lambda_{em} = 590$ and ~620 nm respectively (Fig. 3). Analysis of samples of [Ir(ppy)$_2$(pytr-Sq-girentuximab)] and [Ir(piq)$_2$(pytr-Sq-girentuximab)] by size-exclusion chromatography confirmed that the conjugates are stable for at least 8 months when stored in 0.9% saline at 4 °C in a fridge. The emission spectra of both conjugates do not change when challenged with a mixture of cysteine and histidine (5 mM) for at least 4 hours suggesting the conjugates are likely to be stable with respect to ligand exchange in the presence of proteins present *in vivo* (Fig. S14).

Cellular uptake and phototoxicity of [Ir(C^N)$_2$(pytr-Sq-girentuximab)] in HT-29 cells

The cellular uptake of [Ir(piq)$_2$(pytr-Sq-girentuximab)] in HT-29 cells, which overexpress CAIX,[22,29,30] was investigated by confocal microscopy. The lower energy of the MLCT for [Ir(piq)$_2$(pytr-Sq-girentuximab)], when compared to [Ir(ppy)$_2$(-pytr-Sq-girentuximab)], allows excitation at $\lambda_{ex} = 458$ nm, minimising autofluorescence. HT-29 cells were treated with [Ir(piq)$_2$(pytr-Sq-girentuximab)] and Hoechst 33342 (nuclear stain) for 1 h. The media was exchanged and then the cells were imaged with live cell scanning confocal fluorescence microscopy and transmitted light/bright field imaging (Fig. 4a). Inspection of the images reveals the conjugate has internalised with a distinct perinuclear localisation. Internalisation and perinuclear localisation is consistent with earlier studies that use secondary immunofluorescence to demonstrate that girentuximab internalizes by clathrin-coated vesicles, escapes degradation in lysosomes and enters the recycling pathway by the perinuclear compartment.[29]

The cytotoxicity and photocytotoxicity of both [Ir(C^N)$_2$(pytr-Sq-girentuximab)] complexes to HT-29 cells were investigated using standard 3-(4,5-dimethylthiazol-2-yl)-2,5-diphenyltetrazolium bromide (MTT) cell viability assays. Cells were incubated with serial dilutions of the antibody conjugates for 1 h then washed to remove any unbound conjugate. Following a media change, cells were incubated overnight before being incubated with MTT for 2 h. After solubilisation of the purple formazan crystals, the absorbance at $\lambda = 590$ nm was measured. Both girentuximab conjugates were not cytotoxic at concentrations of at least 26 μM in the dark. In contrast, in cells that had been treated with [Ir(piq)$_2$(pytr-Sq-girentuximab)], irradiation with light ($\lambda = 420$ nm, 26.84 mW cm^{-2}, 30 min) induced dose-dependent toxicity with an IC$_{50}$ value of 1.8 μM (Fig. 4b). Irradiation of cells treated with [Ir(ppy)$_2$(pytr-Sq-girentuximab)] did not induce cytotoxicity presumably because the 420 nm irradiation light does not overlap with the MLCT transition (380 nm).

In previous work, a conjugate of girentuximab labelled with both γ-emitting indium-111 and IRDye800CW was evaluated as an interoperative probe for surgical resection in patients with clear cell renal cell carcinoma.[6,31] The emission of the conjugate was found to assist in identification of the tumour margins.[6] In another related approach, a near-infrared fluorophore was linked to either acetazolamide or 6-aminosaccharin, small molecules that bind to CAIX.[30] These compounds allowed visualization of hypoxic regions of solid tumours in mouse models.

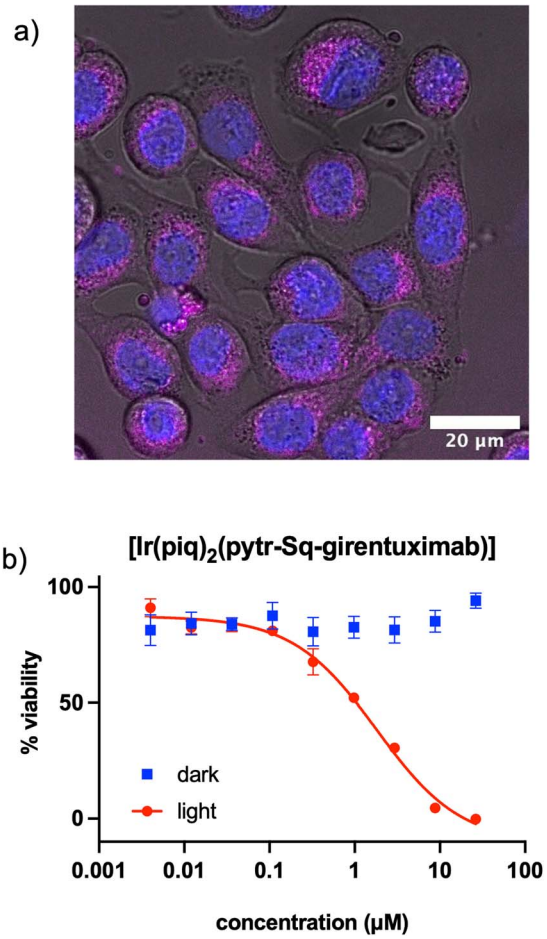

Fig. 4 (a) Confocal microscope image of HT-29 cells treated with [Ir(piq)$_2$(pytr-Sq-girentuximab)] (pink, $\lambda_{ex} = 458$ nm) and Hoescht 33342 (nuclear stain, blue, $\lambda_{ex} = 405$ nm) overlayed on a bright-field image. (b) dose–response curves for [Ir(piq)$_2$(pytr-Sq-girentuximab)] in HT-29 cells either in the dark (blue) or with irradiation (red, $\lambda_{ex} = 420$ nm, 26.84 mW cm^{-2}, 30 min).

The excitation and emission energies from the iridium(III) complexes described in this manuscript can be tuned by changing the energy of the MLCT by increasing the aromatic conjugation in the cyclometalating ligand. The use of phosphorescent metal complexes for photodynamic detection of tumour margins has potential advantages when compared to the use of organic fluorophores, including large Stokes shifts, minimised inner-filter effects, relatively long emission lifetimes and a resistance to photobleaching. The iridium(III) complexes described here are not toxic in the dark but upon irradiation with visible light generate singlet oxygen and subsequent phototoxicity. Future work will investigate the cellular mechanisms of phototoxicity as it is of considerable interest that photodynamic therapy with phosphorescent rhenium(I) complexes induces immune responses.[32,33]

Conclusions

A new bidentate 2-pyridyl-1,2,3-triazole ligand with a relatively long polyethylene glycol linker (PEG_7) with a terminal squaramide ethyl ester functional group is used to make phosphorescent iridium(III) antibody conjugates. The new iridium(III) complexes were reacted with girentuximab and the squaramide ethyl ester functional group reacts with lysine residues in the antibody to attach the iridium(III) complexes through stable vinylogous amide linkages. The iridium(III)-girentuximab conjugates retain affinity for CAIX. The cellular uptake of [Ir(piq)$_2$(pytr-Sq-girentuximab)] was demonstrated using confocal microscopy. [Ir(piq)$_2$(pytr-Sq-girentuximab)] is not toxic to HT-29 cells that over express CAIX, but irradiation with visible light results in dose dependent cytotoxicity. It is feasible that [Ir(piq)$_2$(pytr-Sq-girentuximab)] could be of use for phosphorescent detection of CAIX positive tumour tissue to guide surgical resection as well as CAIX targeted photodynamic therapy. The approach described here could be used to prepare phosphorescent conjugates with other tumour targeting antibodies.

Author contributions

The manuscript was written through contributions of all authors. All authors have given approval to the final version of the manuscript.

Conflicts of interest

P. S. D. has a financial interest in Telix Pharmaceuticals, a company who has an interest in intellectual property relating to the girentuximab antibody used in this work. The other authors have no conflicts to declare. The University of Melbourne has collaborative research agreements with Telix Pharmaceuticals that are not directly related to this work.

Data availability

All experimental data is provided within the manuscript or the supplementary information (SI). Supplementary information is available. See DOI: https://doi.org/10.1039/d5sc07715j.

Acknowledgements

This research was funded by the Australian Research Council (DP Scheme and ARC Industrial Transformation Training Centre for the Development of Advanced Radiochemical Technologies (DART) IC230100046) and the National Health and Medical Research Council (Australia). We acknowledge the Bio21 Mass Spectrometry and Proteomics Facility and the Biological Optical Microscopy Platform at the University of Melbourne for instrumentation and technical support. Financial support from the Australian Cancer Research Foundation supported the purchase of an NMR spectrometer used in this work. Dr Asif Noor (University of Melbourne) is thanked for his expertise and assistance in the ELISA assay. Girentuximab was provided by Telix Pharmaceuticals. Dr Michael Wheatcroft (Telix Pharmaceuticals) is thanked for his support of this work. EM acknowledges funding from an RTP (PhD) scholarship and a Norma Hilda Schuster (nee Swift) scholarship. Professor Kenneth Kam-Wing Lo and Prof Sherri A. McFarland are thanked for generous advice on phototoxicity measurements.

Notes and references

1 F. W. B. van Leeuwen, T. Buckle, M. N. van Oosterom and D. D. D. Rietbergen, *J. Nucl. Med.*, 2024, **65**, 1505–1511.
2 P. A. Sutton, M. A. van Dam, R. A. Cahill, S. Mieog, K. Polom, A. L. Vahrmeijer and J. van der Vorst, *BJS Open*, 2023, **7**, zrad049.
3 J. S. D. Mieog, F. B. Achterberg, A. Zlitni, M. Hutteman, J. Burggraaf, R.-J. Swijnenburg, S. Gioux and A. L. Vahrmeijer, *Nat. Rev. Clin. Oncol.*, 2022, **19**, 9–22.
4 S. Giuliani, I. Paraboschi, A. McNair, M. Smith, K. S. Rankin, D. S. Elson, V. Paleri, D. Leff, G. Stasiuk and J. Anderson, *Cancers*, 2024, 16.
5 P. Dell'Oglio, P. Meershoek, T. Maurer, E. M. K. Wit, P. J. van Leeuwen, H. G. van der Poel, F. W. B. van Leeuwen and M. N. van Oosterom, *Eur. Urol.*, 2021, **79**, 124–132.
6 M. C. Hekman, M. Rijpkema, C. H. Muselaers, E. Oosterwijk, C. A. Hulsbergen-Van de Kaa, O. C. Boerman, W. J. Oyen, J. F. Langenhuijsen and P. F. Mulders, *Theranostics*, 2018, **8**, 2161–2170.
7 P. Dell'Oglio, D. M. van Willigen, M. N. van Oosterom, K. Bauwens, F. Hensbergen, M. M. Welling, H. van der Stadt, E. Bekers, M. Pool, P. van Leeuwen, T. Maurer, F. W. B. van Leeuwen and T. Buckle, *EJNMMI Res.*, 2022, **12**, 14.
8 J. Jiao, J. Zhang, W. Wen, W. Qin and X. Chen, *Theranostics*, 2024, **14**, 2736–2756.
9 L. C.-C. Lee and K. K.-W. Lo, *J. Am. Chem. Soc.*, 2022, **144**, 14420–14440.
10 Y. Wu, S. Li, Y. Chen, W. He and Z. Guo, *Chem. Sci.*, 2022, **13**, 5085–5106.
11 X. Wang, J. Peng, C. Meng and F. Feng, *Chem. Sci.*, 2024, **15**, 12234–12257.
12 P. Konda, L. M. Lifshits, J. A. Roque III, H. D. Cole, C. G. Cameron, S. A. McFarland and S. Gujar, *OncoImmunology*, 2021, **10**, 1863621–1863626.
13 Y. Zhang, B.-T. Doan and G. Gasser, *Chem. Rev.*, 2023, **123**, 10135–10155.
14 S. Monro, K. L. Colon, H. Yin, J. Roque, P. Konda, S. Gujar, R. P. Thummel, L. Lilge, C. G. Cameron and S. A. McFarland, *Chem. Rev.*, 2019, **119**, 797–828.
15 T. U. Connell, J. M. White, T. A. Smith and P. S. Donnelly, *Inorg. Chem.*, 2016, **55**, 2776–2790.
16 T. U. Connell, J. L. James, A. R. White and P. S. Donnelly, *Chem.–Eur. J.*, 2015, **21**, 14146–14155.
17 S. E. Rudd, P. Roselt, C. Cullinane, R. J. Hicks and P. S. Donnelly, *Chem. Commun.*, 2016, **52**, 11889–11892.
18 S. E. Rudd, J. K. Van Zuylekom, A. Raicevic, L. A. Pearce, C. Cullinane, C. C. Williams, T. E. Adams, R. J. Hicks and P. S. Donnelly, *Chem. Sci.*, 2021, **12**, 9004–9016.

19 K. A. Morgan, C. W. Wichmann, L. D. Osellame, Z. Cao, N. Guo, A. M. Scott and P. S. Donnelly, *Chem. Sci.*, 2024, **15**, 3372–3381.
20 S. E. Rudd, A. Noor, K. A. Morgan and P. S. Donnelly, *Acc. Chem. Res.*, 2024, **57**, 1421–1433.
21 B. Shuch, A. J. Pantuck, J.-C. Bernhard, M. A. Morris, V. Master, A. M. Scott, C. van Praet, C. Bailly, B. Önal, T. Aksoy, R. Merkx, D. M. Schuster, S. T. Lee, N. Pandit-Taskar, A. C. Fan, P. Allman, K. Schmidt, L. Tauchmanova, M. Wheatcroft, C. Behrenbruch, C. R. W. Hayward and P. Mulders, *Lancet Oncol.*, 2024, **25**, 1277–1287.
22 A. Noor, E. R. McGowan, J. K. Van Zuylekom, C. Cullinane, P. D. Roselt, R. J. Hicks, M. P. Wheatcroft and P. S. Donnelly, *EJNMMI Radiopharm. Chem.*, 2024, **9**, 80.
23 C. H. J. Muselaers, M. J. Boers-Sonderen, T. J. van Oostenbrugge, O. C. Boerman, I. M. E. Desar, A. B. Stillebroer, S. F. Mulder, C. M. L. van Herpen, J. F. Langenhuijsen, E. Oosterwijk, W. J. G. Oyen and P. F. A. Mulders, *Eur. Urol.*, 2016, **69**, 767–770.
24 N. R. Babij, E. O. McCusker, G. T. Whiteker, B. Canturk, N. Choy, L. C. Creemer, C. V. D. Amicis, N. M. Hewlett, P. L. Johnson, J. A. Knobelsdorf, F. Li, B. A. Lorsbach, B. M. Nugent, S. J. Ryan, M. R. Smith and Q. Yang, *Org. Process Res. Dev.*, 2016, **20**, 661–667.
25 S. Liu, P. Müller, M. K. Takase and T. M. Swager, *Inorg. Chem.*, 2011, **50**, 7598–7609.
26 E. Orselli, R. Q. Albuquerque, P. M. Fransen, R. Fröhlich, H. M. Janssen and L. De Cola, *J. Mater. Chem.*, 2008, **18**, 4579–4590.
27 D. Abad-Montero, A. Gandioso, E. Izquierdo-García, S. Chumillas, A. Rovira, M. Bosch, M. Jordà-Redondo, D. Castaño, J. Bonelli, V. V. Novikov, A. Deyà, J. L. Hernández, J. Galino, M. E. Alberto, A. Francés-Monerris, S. Nonell, G. Gasser and V. Marchán, *J. Am. Chem. Soc.*, 2025, **147**, 7360–7376.
28 P.-N. Lai, C. H. Brysacz, M. K. Alam, N. A. Ayoub, T. G. Gray, J. Bao and T. S. Teets, *J. Am. Chem. Soc.*, 2018, **140**, 10198–10207.
29 M. Zatovicova, L. Jelenska, A. Hulikova, P. Ditte, Z. Ditte, L. Csaderova, E. Svastova, W. Schmalix, V. Boettger, P. Bevan, J. Pastorek and S. Pastorekova, *Int. J. Oncol*, 2014, **45**, 2455–2467.
30 S. M. Mahalingam, H. Chu, X. Liu, C. P. Leamon and P. S. Low, *Bioconjugate Chem.*, 2018, **29**, 3320–3331.
31 M. Rijpkema, D. L. Bos, A. S. Cornelissen, G. M. Franssen, D. M. Goldenberg, W. J. Oyen and O. C. Boerman, *Mol. Imaging*, 2015, **14**, 7290.
32 X. Su, W.-J. Wang, Q. Cao, H. Zhang, B. Liu, Y. Ling, X. Zhou and Z.-W. Mao, *Angew. Chem., Int. Ed.*, 2022, **61**, e202115800.
33 D. Li, G. Wen, H. Wang, Q. Ren, D. Wang, A. Dao, H. Huang and P. Zhang, *J. Med. Chem.*, 2025, **68**, 3749–3763.